Arthritis & Rheumatology
Vol. 0, No. 0, Month 2019, pp 1–11
DOI 10.1002/art.40877

American College of Rheumatology
Empowering Rheumatology Professionals

Amelioration of Autoimmune Arthritis in Mice Treated With the DNA Methyltransferase Inhibitor 5'-Azacytidine

Dániel M. Tóth,[1] Timea Ocskó,[1] Attila Balog,[2] Adrienn Markovics,[1] Katalin Mikecz,[1] László Kovács,[2] Meenakshi Jolly,[1] Aleksandra A. Bukiej,[1] Andrew D. Ruthberg,[1] András Vida,[1] Joel A. Block,[1] Tibor T. Glant,[1] and Tibor A. Rauch[3]

Objective. Disease-associated, differentially hypermethylated regions have been reported in rheumatoid arthritis (RA), but no DNA methyltransferase inhibitors have been evaluated in either RA or any animal models of RA. The present study was conducted to evaluate the therapeutic potential of 5′-azacytidine (5′-azaC), a DNA methyltransferase inhibitor, and explore the cellular and gene regulatory networks involved in the context of autoimmune arthritis.

Methods. A disease-associated genome-wide DNA methylation profile was explored by methylated CpG island recovery assay–chromatin immunoprecipitation (ChIP) in arthritic B cells. Mice with proteoglycan-induced arthritis (PGIA) were treated with 5′-azaC. The effect of 5′-azaC on the pathogenesis of PGIA was explored by measuring serum IgM and IgG1 antibody levels using enzyme-linked immunosorbent assay, investigating the efficiency of class-switch recombination (CSR) and *Aicda* gene expression using real-time quantitative polymerase chain reaction, monitoring germinal center (GC) formation by immunohistochemistry, and determining alterations in B cell subpopulations by flow cytometry. The 5′-azaC–induced regulation of the *Aicda* gene was explored using RNA interference, ChIP, and luciferase assays.

Results. We explored arthritis-associated hypermethylated regions in mouse B cells and demonstrated that DNA demethylation had a beneficial effect on autoimmune arthritis. The 5′-azaC–mediated demethylation of the epigenetically inactivated *Ahr* gene resulted in suppressed expression of the *Aicda* gene, reduced CSR, and compromised GC formation. Ultimately, this process led to diminished IgG1 antibody production and amelioration of autoimmune arthritis in mice.

Conclusion. DNA hypermethylation plays a leading role in the pathogenesis of autoimmune arthritis and its targeted inhibition has therapeutic potential in arthritis management.

INTRODUCTION

Rheumatoid arthritis (RA) is a systemic inflammatory autoimmune disorder that primarily leads to joint destruction. B cells play an indispensable role in its initiation via the production of high-affinity autoantibodies. It has recently been suggested that dysregulation of the B cell epigenome can contribute to this antibody production (1).

Currently, there is no cure for RA, but treatments can provide alleviation of symptoms and modify disease progression. In most cases, the optimal treatment can only be achieved through a combination of different drugs (2). When a combination of traditional disease-modifying antirheumatic drugs, nonsteroidal antiinflammatory drugs, and/or low-dose glucocorticoids does not provide a satisfactory response, highly specific biologic agents are introduced into the treatment regimen (2,3). Highly effective epigenetic enzyme inhibitors have already been developed, and their therapeutic potential has been demonstrated in cancer (4). However, no such drug is currently used to treat RA (5). Epigenetic enzyme targeting drugs represent a novel

Supported by the NIH (grants R01-AR-059356 and R01-AR-062991 to Dr. Glant and R21-AR-064948 to Dr. Rauch). Dr. Balog is supported by the Hungarian Academy of Sciences (the János Bolyai Scholarship).

[1]Dániel M. Tóth, PhD, Timea Ocskó, MSc, Adrienn Markovics, MD, PhD, Katalin Mikecz, MD, PhD, Meenakshi Jolly, MD, Aleksandra A. Bukiej, MD, Andrew D. Ruthberg, MD, András Vida, PhD, Joel A. Block, MD, Tibor T. Glant, MD, PhD: Rush University Medical Center, Chicago, Illinois; [2]Attila Balog, MD, PhD, László Kovács, MD, PhD: Albert Szent-Györgyi Clinical Center, Szeged, Hungary; [3]Tibor A. Rauch, PhD: Rush University Medical Center, Chicago, Illinois, and University of Pécs, Pécs, Hungary.

Dr. Rauch holds a patent for a method of detecting methylated CpG islands (US patent application no. 7,425,415). No other disclosures relevant to this article were reported.

Address correspondence to Tibor A. Rauch, PhD, Department of Medical Biology, School of Medicine, University of Pécs, Pécs, 48-as tér 1, 7622, Hungary. E-mail: Tibor.Rauch@aok.pte.hu.

Submitted for publication October 19, 2018; accepted in revised form February 28, 2019.

approach that might replace or be used in combination with conventional arthritis therapies to achieve more effective arthritis management.

DNA methylation, one of the most common epigenetic modifications, is catalyzed by DNA methyltransferases and associated with gene silencing when it takes place in promoter regions (6). Recent studies have shown that RA pathogenesis is associated with DNA methylome changes similarly to carcinogenesis. In both diseases characteristic global DNA hypomethylation (decreased methylation) events affecting intergenic and intragenic regions (7–9) and de novo hypermethylated (increased methylation) promoters have been described (8,10). Induced demethylation of disease-specific hypermethylated promoters using DNA methyltransferase inhibitors, such as 5′-azacytidine (5′-azaC), can rescue the epigenetically inactivated genes, resulting in impaired disease progression (11,12). However, the significance of DNA hypermethylation in RA pathogenesis has been shown only indirectly (13). We hypothesized that locus-specific hypermethylation in B cells may play a role in arthritis pathogenesis and that DNA methylation inhibitors may have therapeutic potential in RA.

Herein, we report that low-dose 5′-azaC treatment has a notable effect on disease progression in proteoglycan-induced arthritis (PGIA), a murine model of RA (14). The 5′-azaC–mediated suppressive effect is due to transcriptional silencing of activation-induced cytidine deaminase (AID), an enzyme responsible for multiple catalytic steps of high-affinity antibody maturation encompassing class-switch recombination (CSR) and somatic hypermutation (15,16). Furthermore, AID plays a pivotal role in germinal center (GC) formation (17), the site of autoantibody production in secondary lymphoid organs (18). We demonstrate that aryl hydrocarbon receptor (AHR) transcription factor, which is known to be involved in B cell differentiation (19) and directly regulates *Aicda* expression (20), is rescued from arthritis-associated promoter hypermethylation in B cells after 5′-azaC treatment and contributes to the suppression of antibody production. These data promote consideration of epigenetic drugs in arthritis therapy.

MATERIALS AND METHODS

Methylated CpG island recovery assay (MIRA). MIRA–chromatin immunoprecipitation (ChIP) was performed as previously described. MIRA-enriched DNA fractions were analyzed by quantitative polymerase chain reaction (qPCR) wherein the *Xist* promoter and mouse *Gapdh* or human *TBP* promoters were used as positive and negative controls, respectively (Supplementary Table 1, available on the *Arthritis & Rheumatology* web site at http://onlinelibrary.wiley.com/doi/10.1002/art.40877/abstract). Measured C_t values were compared to negative control promoter–related C_t values as 1-fold baseline methylation level. DNA methylation raw data files are accessible at NCBI GEO (accession no. GSE98939).

Gene expression analysis using Agilent microarray platforms. RNA sample labeling, array hybridization, and primary data analysis were performed by Arraystar. Microarray data are available from the NCBI GEO database (accession no. GSE98932).

Induction and assessment of PGIA in mice and 5'-azaC treatment. To induce PGIA, 3-month old female wild-type BALB/c mice (Charles River) were immunized intraperitoneally with human PG as previously described (14). At disease onset, the degree of arthritis in each paw was visually scored for redness and swelling on a scale of 0–4 every other day (21). The scoring was performed by one individual (TTG) in a blinded manner. Mice with a score of ≥1 on at least 1 limb were divided into 2 groups. The 5′-azaC–treated mice with PGIA received 2 mg/kg of 5′-azaC (Sigma-Aldrich) IP every other day for either 2 weeks or 4 weeks. The 5′-azaC was freshly dissolved at 0.5 mg/ml concentration in saline solution. The control mice with PGIA received saline solution alone. For in vitro tests, samples were obtained from the mice treated for 2 weeks. The animal studies were reviewed and approved by the Institutional Animal Care and Use Committee (IACUC) of Rush University Medical Center (IACUC # 15–065).

Histologic analysis. Tissue sections from mouse hind limbs were prepared, processed, examined, and photographed as previously described (21).

Enzyme-linked immunosorbent assay (ELISA). Briefly, IgM isotype control (catalog no. 02-6800; ThermoFisher) or mouse purified IgG1 (0.025 μg/well) was coated onto an ELISA plate. IgM horseradish peroxidase (HRP) antibody (catalog no. 04-6820; ThermoFisher) was diluted to 1:2,000 in phosphate buffered saline (PBS) and added to serum samples diluted 1:100. IgG1 HRP antibody (catalog no. 559626; BD Biosciences) was diluted to 1:40,000 and added to serum samples diluted 1:160,000. For no-serum control (NSC), diluted antibodies were incubated in PBS. After a 1-hour incubation at room temperature, samples were added to coated wells and incubated for an additional hour at room temperature. After washes, the color reaction was developed and the optical density (OD) was read using a Synergy 2 ELISA reader. The OD of the NSC well was set to 100% binding, and the percentage of inhibition was calculated according to the formula % inhibition = $100–[(OD_{sample} \times 100)/OD_{NSC}]$. To measure serum levels of the cytokine interleukin-4 (IL-4), a mouse IL-4 ELISA kit (catalog no. 555232; BD Biosciences) was used according to the recommendations of the manufacturer.

Isolation of B cells and human peripheral blood mononuclear cells (PBMCs). Mouse spleen cells were isolated, and an immunomagnetic selection kit (StemCell) was used for negative B cell selection, according to the recommendations

of the manufacturer. Peripheral blood samples were obtained from consenting treatment-naive RA patients and from consenting healthy individuals (Supplementary Table 2, available on the *Arthritis & Rheumatology* web site at http://onlinelibrary.wiley.com/doi/10.1002/art.40877/abstract) at Albert Szent-Györgyi Clinical Center and Rush University Medical Center under Ethics Committee– and IRB-approved protocols (Hungarian ETT TUKEB905/PI/09 and RUMC 13082202-IRB01). PBMCs were separated on a Ficoll density gradient within 1 hour of blood draw, and were then stored in RNAlater solution (ThermoFisher) until RNA and DNA preparation. Human B cells were isolated from peripheral blood using a negative immunomagnetic selection kit (StemCell) according to the recommendations of the manufacturer.

RNA isolation, complementary DNA (cDNA) synthesis, and real-time qPCR. Total RNA preparation, cDNA synthesis, and real-time qPCR were conducted as previously described (17). Measured C_t values were normalized to *Hprt1* (mouse samples) or β-actin (human samples). Relative expression was calculated using CFX Manager software (Bio-Rad). The primers used are listed in Supplementary Table 1, available on the *Arthritis & Rheumatology* web site at http://onlinelibrary.wiley.com/doi/10.1002/art.40877/abstract.

Digestion-circulation qPCR. Digestion-circulation qPCR was performed based on the method described by Lumsden et al (22) with modifications. Quantitative PCR was used to quantify circulated DNA products. The qPCR was performed in 25 μl final volume using 5 μl circulated DNA, SsoAdvanced Universal SYBR Green Supermix (Bio-Rad), and primers (Supplementary Table 1) at 0.5 μ*M* final concentration. The qPCR conditions were as follows: 94°C for 2 minutes, 40 cycles at 94°C for 8 seconds, and 62°C for 30 seconds. Circulated nicotinic acetylcholine receptor (nAChR) DNA was used for normalization. Relative quantities of IgG1-specific recombinant DNA (Sμ–Sγ1) were calculated by $2^{-\Delta Ct}$ equation, where $\Delta Ct = Ct_{S\mu-S\gamma1} - Ct_{nAChR}$.

Flow cytometric analysis. Erythrocytes were lysed from mouse spleen and bone marrow (BM) cells by hypotonic buffer, then Fc receptors (FcR) were blocked with TruStain FcX anti-mouse CD16/CD32 (catalog no. 101320; BioLegend) and surface antigens were stained with fluorescence-labeled antibodies (Supplementary Table 3, available on the *Arthritis & Rheumatology* web site at http://onlinelibrary.wiley.com/doi/10.1002/art.40877/abstract). Data acquisition and analysis were performed using a FACSCanto II instrument and BD FACSDiva software (version 5.0).

Immunohistochemistry. Mouse spleens and lymph nodes were embedded and snap-frozen in Tissue-Tek OCT compound (Sakura Finetek), cut on a Microm HM 550 cryostat (Microm International), and stored at –20°C until used. Sections were fixed by cold 100% acetone (Sigma-Aldrich) and blocked with 1% normal goat serum (ThermoFisher) in PBS, then immunostained with fluorescence-labeled antibodies (Supplementary Table 3) for 1 hour. Stained sections were post-fixed in 10% formalin and images were captured on a Zeiss LSM 700 confocal microscope and analyzed with Zen 2.0 software (Zeiss).

Cell cultures and in vitro 5'-azaC treatment. A20 BALB/c mouse B lymphoma and HEK 293T cell lines were purchased from ATCC and were maintained in Dulbecco's modified Eagle's medium (Sigma-Aldrich) supplemented with 10% fetal bovine serum (FBS; HyClone) and antibiotics. The human B cell line GM12878 was purchased from the Coriell Institute of Aging Cell Repository and was cultured in RPMI 1640 medium (Lonza) supplemented with 15% FBS and antibiotics. All cells were maintained under standard culture conditions.

The 5′-azaC was dissolved in DMSO at a 10 m*M* concentration and stored at –20°C until used. A20 cells were plated into 6-well plates (2×10^5 cell/ml) in medium supplemented with 5′-azaC at a 10 μ*M* final concentration. Control samples were treated with DMSO at a 0.1% final concentration. Cell cultures were incubated for 24, 48, or 72 hours. Media with the same reagents were replaced with fresh media every 24 hours.

Western blot analyses. A20 cells were treated with 5′-azaC for 48 hours, and then nuclear and cytoplasmic extracts were prepared using a Nuclei EZ Prep kit (Sigma-Aldrich) according to the manufacturer's instructions. Protein concentrations were determined using a BCA Protein Assay kit (ThermoFisher) and a Synergy 2 ELISA reader (BioTek Instruments). Protein extracts were separated on 4–20% sodium dodecyl sulfate–polyacrylamide gels (Bio-Rad), blotted onto Immuno-Blot membranes (Bio-Rad), then blocked with Tris buffered saline–0.05% Tween 20 containing 3% nonfat milk, and incubated with the following primary antibodies at 4°C overnight: anti-*Ahr* (1:500) (catalog no. GTX22769; GeneTex), anti-*Aicda* (1:625) (catalog no. ZA001; ThermoFisher), antilamin β (1:300) (catalog no. sc6217; Santa Cruz Biotechnology), and anti-GAPDH (1:10,000) (catalog no. G9545; Sigma-Aldrich). HRP-conjugated secondary antibodies were purchased from Santa Cruz Biotechnology. Pierce ECL Western Blotting Substrate (ThermoFisher) was used to generate a chemiluminescent signal, which was detected by radiography and developed in an Alphatek AX200 machine.

RNA interference study. An *Ahr*-specific short hairpin RNA (shRNA) sequence (Supplementary Table 1) was inserted into the pU6Abase vector (23) downstream of the human U6 promoter (pU6AshRNA). Exponentially growing A20 cells (10^7) were suspended in electroporation buffer (20 m*M* HEPES, 135 m*M* KCl, 2 m*M* $MgCl_2$, and 0.5% Ficoll 400, pH 7.6) together with 20 μg plas-

mid DNA. Electroporation was carried out using 940 volts/cm and 950 μF in a Gene Pulser II machine (Bio-Rad). Cells were plated onto 6-well plates and after a 12-hour incubation they were treated with 10 μ*M* 5′-azaC. Twenty-four hours later the cells were resuspended in fresh tissue culture medium supplemented with 10 μ*M* 5′-azaC and incubated for an additional 24 hours before isolation of total RNA. The pU6Abase without insert was used as control.

ChIP assay. ChIP assay was performed on A20 cells after treatment with 10 μ*M* 5′-azaC for 48 hours. For IP, 50 μg precleared chromatin was incubated with 20 μg rabbit polyclonal anti-*Ahr* antibody (catalog no. sc5579; Santa Cruz Biotechnology) or incubated without antibody (mock). DNA–*Ahr* antibody complexes were collected using magnetic beads. DNA–*AHR* antibody complexes were eluted and reverse crosslinked as input. One microliter of the eluted DNA fraction was used for qPCR in which region-specific primers were used (Supplementary Table 4, available on the *Arthritis & Rheumatology* web site at http://onlinelibrary.wiley.com/doi/10.1002/art.40877/abstract). Quantitative data were calculated by the $\Delta\Delta C_t$ method and presented as fold enrichment compared to the values for the mock-treated samples.

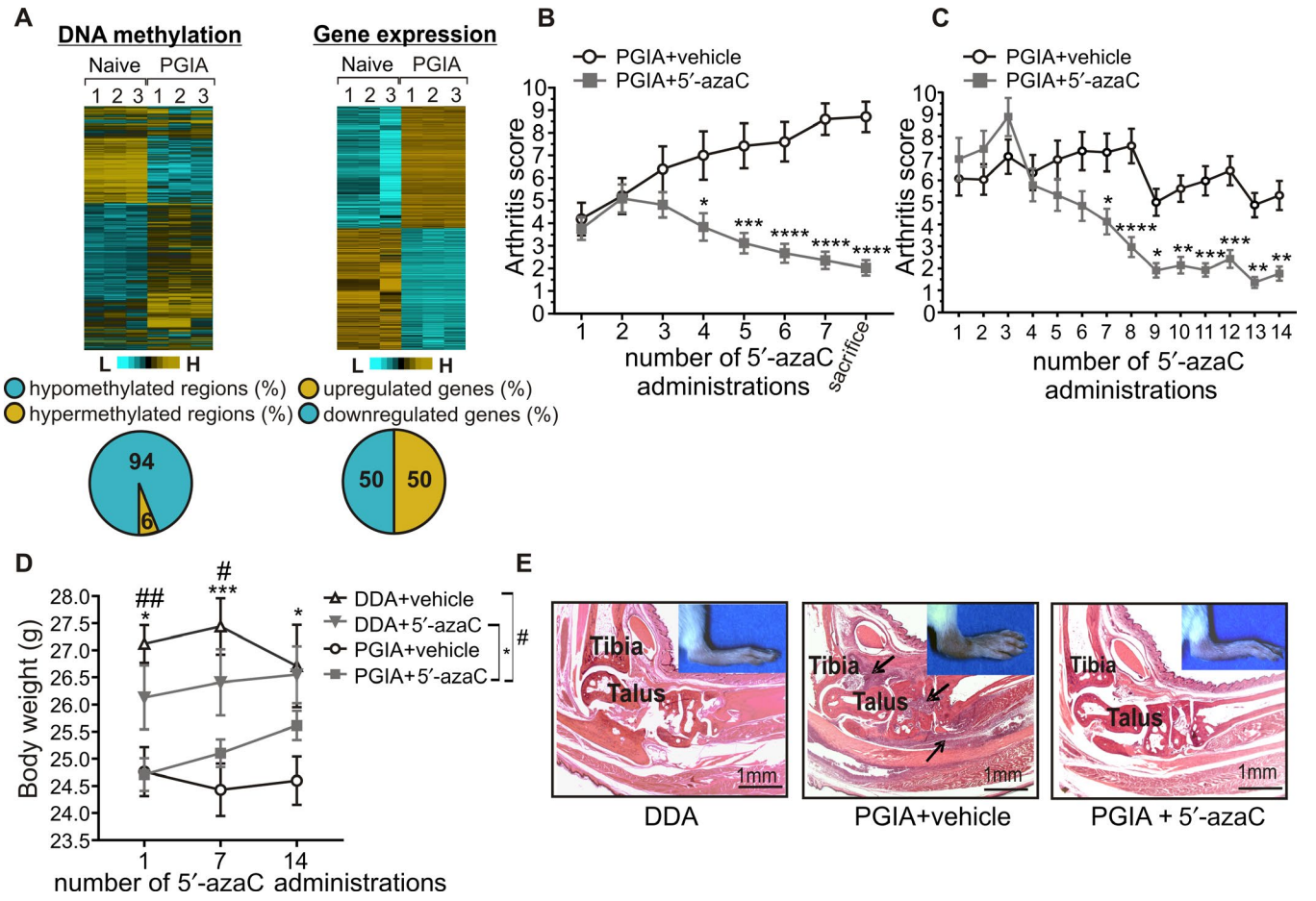

Figure 1. Amelioration of autoimmune arthritis in mice treated with 5′-azacytidine (5′-azaC). **A**, Heatmap of differentially methylated regions (left) and arthritis-associated gene expression changes (right) in B cells from naive mice (n = 3) and mice with proteoglycan-induced arthritis (PGIA; n = 3). Pie charts depict the methylation pattern (left) and gene expression pattern (right) of the annotated sites and genes in samples from mice with PGIA. **B** and **C**, Arthritis scores for mice with PGIA treated with vehicle (saline) (n = 19 in **B** and 24 in **C**) and mice with PGIA treated with 5′-azaC (n = 21 in **B** and 28 in **C**) intraperitoneally every other day for 2 weeks (**B**) or 4 weeks (**C**). Values are the mean ± SEM. * = $P \leq 0.05$; ** = $P \leq 0.01$; *** = $P \leq 0.001$; **** = $P \leq 0.0001$ versus vehicle, by two-way analysis of variance (ANOVA) with Sidak's test. **D**, Body weight of mice injected with dimethyldioctadecylammonium bromide (DDA) adjuvant and treated with vehicle (n = 10), mice injected with DDA adjuvant and treated with 5′-azaC (n = 10), mice with PGIA treated with vehicle (n = 24), and mice with PGIA treated with 5′-azaC (n = 28). Values are the mean ± SEM. # = $P \leq 0.05$; ## = $P \leq 0.01$, mice injected with DDA treated with vehicle versus mice with PGIA treated with vehicle; * = $P \leq 0.05$; *** = $P \leq 0.001$, mice injected with DDA treated with 5′-azaC versus mice with PGIA treated with 5′-azaC, by two-way ANOVA with Sidak's test. **E**, Representative images of histopathologic features of hematoxylin and eosin–stained ankle joints from mice injected with DDA adjuvant, mice with PGIA treated with vehicle, and mice with PGIA treated with 5′-azaC. **Arrows** indicate bone-eroding inflammatory tissue. Color figure can be viewed in the online issue, which is available at http://onlinelibrary.wiley.com/doi/10.1002/art.40877/abstract.

Luciferase assay. Briefly, the mouse *Aicda* minimal promoter and the longer variant (including region 13, named pGL4.1-Aicda-p+13r) or the shorter variant (without region 13, named pGL4.1-Aicda-p+Δ13r) of the intronic region of *Aicda* was cloned into pGL4.1 (Promega). A reporter plasmid with a human *AHR*-overexpressing plasmid (pCMV-hAHR; OriGene) or with a control vector (pCMV-EGFP; Addgene) were cotransfected into HEK 293T cells. Twenty-four hours after transfection, luciferase activity was measured. The relative luciferase activity was calculated by normalization of measured relative luminescence units to protein concentrations.

Statistical analysis. All statistical analyses were performed using GraphPad Prism software, version 7.04. Results are reported as the mean ± SEM. If the significance level for the pretest for normality (Shapiro-Wilk) was less than 0.05, the Mann-Whitney U test was used. If the significance level for the pretest was greater than 0.05, Student's unpaired 2-tailed *t*-test was used. Comparisons of more than 2 groups were performed by one-way analysis of variance (ANOVA), and groups affected by 2 factors were compared by two-way ANOVA followed by Sidak's post hoc comparison. *P* values less than 0.05 were considered significant.

RESULTS

Elimination of PGIA symptoms in mice treated with low doses of a DNA hypomethylating agent. To investigate the role of DNA methylation in RA pathology, we conducted an integrative analysis by exploring genome-wide DNA methylation and accompanying gene expression changes in B cells from mice with PGIA (Figure 1A). We observed dominant arthritis-associated hypomethylation and rare hypermethylation events in the investigated intergenic and intragenic regions in arthritic B cells (Supplementary Table 5, available on the *Arthritis & Rheumatology* web site at http://onlinelibrary.wiley.com/doi/10.1002/art.40877/abstract). However, DNA methylation profile changes were infrequently followed by gene expression changes, implying that most of the methylation events have no direct effects on gene expression.

We recognized that carcinogenesis- and arthritis-associated DNA methylation profile changes are similar in a sense, as both are characterized by dominant genome-wide hypomethylation affecting intergenic and intragenic regions, and infrequent promoter-specific hypermethylation events (24). Accordingly, we hypothesized that a demethylating agent that proved to be effective in cancer treatment could also be effective in arthritis therapy. We treated arthritic mice with low-dose 5′-azaC every other day for 2 weeks, which resulted in gradual reduction of disease severity and halted arthritis progression (Figure 1B). Next, we started 5′-azaC treatment at a more advanced stage of arthritis and continued treatment for 4 weeks, which similarly reduced paw swelling (Figure 1C). Moreover, neither mortality nor toxic effect was observed among these mice. This was confirmed by the increased body weight of 5′-azaC–treated arthritic mice at the fourteenth administration of 5′-azaC (Figure 1D). Furthermore, arthritis-specific massive joint inflammation, synovial pannus formation, cartilage damage, and bone destruction were undetectable by histopathologic analysis in 5′-azaC–treated animals by the end of the study (Figure 1E). These results confirmed our working hypothesis that 5′-azaC–induced DNA demethylation can be an effective approach for the management of autoimmune arthritis.

Attenuated IgG1 antibody production in 5'-azaC–treated mice with PGIA. The lack of joint inflammation prompted us to measure serum levels of IgM and IgG1 antibod-

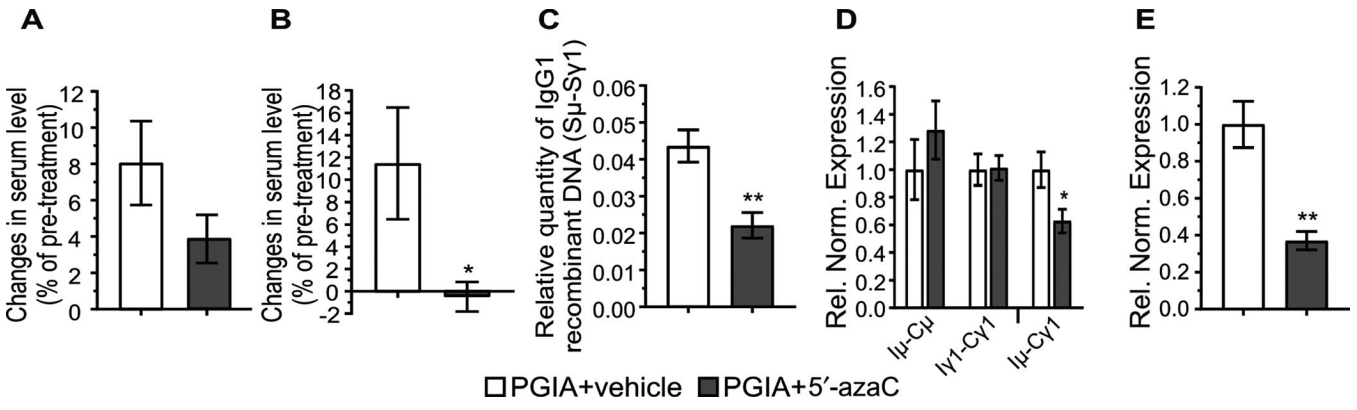

Figure 2. Attenuation of IgG1 production in mice with PGIA treated with 5′-azaC. **A** and **B**, Changes in IgM (**A**) and IgG1 (**B**) antibody levels in mice with PGIA treated with vehicle (n = 8) and mice with PGIA treated with 5′-azaC (n = 8). Sera were collected before the first and after the last 5′-azaC treatment. Values are the percent of pretreatment level. **C**, Relative quantity of IgG1-specific class-switched recombinant genomic DNA (Sμ–Sγ1) in mice with PGIA treated with vehicle (n = 5) and mice with PGIA treated with 5′-azaC (n = 5). **D** and **E,** Relative (rel) normalized (norm) expression of mRNA for germline (Iμ–Cμ and Iγ1–Cγ1) and post-recombination (Iμ–Cγ1) IgG1 (**D**) and for *Aicda* (**E**) in B cells from mice with PGIA treated with vehicle (n = 8) and mice with PGIA treated with 5′-azaC (n = 8). Bars show the mean ± SEM. * = $P \leq 0.05$; ** = $P \leq 0.01$, by the Mann-Whitney U test in **B** and by *t*-test in **C–E**. See Figure 1 for definitions.

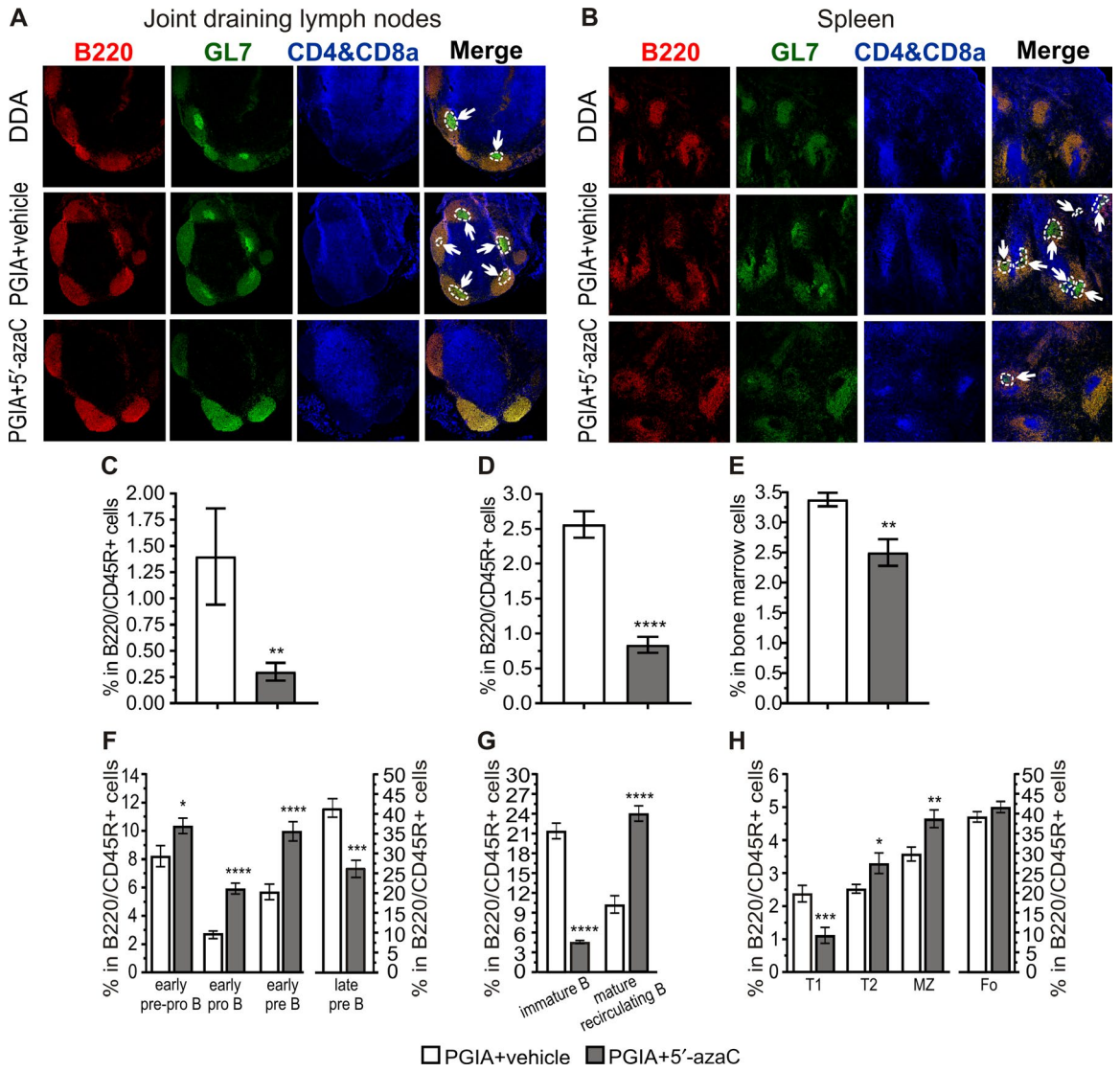

Figure 3. Treatment with 5′-azaC impairs germinal center (GC) formation and shifts former B cell subpopulations in mice with PGIA. **A** and **B**, GCs in the joint draining lymph nodes (**A**) and spleens (**B**) of mice injected with DDA adjuvant, mice with PGIA treated with vehicle, and mice with PGIA treated with 5′-azaC. Red shows follicular B cells (phycoerythrin-conjugated B220/CD45R), green shows GL-7+ B cells (Alexa Fluor 488–conjugated GL-7), and blue shows T cells (biotin-conjugated CD4, biotin-conjugated CD8a, and eFluor 450–conjugated streptavidin). **Arrows** indicate GCs in B cell follicles. Original magnification × 100. **C** and **D**, Percentage of GC B cells, determined by flow cytometry, within B lymphocytes in the lymph nodes (**C**) and spleen (**D**) of mice with PGIA treated with vehicle (n = 8) and mice with PGIA treated with 5′-azaC (n = 8). **E**, Percentage of plasma cells, determined by flow cytometry, within bone marrow cells from mice with PGIA treated with vehicle (n = 5) and mice with PGIA treated with 5′-azaC (n = 5). **F–H**, Percentage of early prepro–B cells, early pro–B cells, early pre–B cells, and late precursor B cells (**F**), immature and mature recirculating B cells (**G**), and transitional type 1 (T1), T2, marginal zone (MZ), and follicular (Fo) B cells (**H**), determined by flow cytometry, within B lymphocytes in the bone marrow (**F** and **G**) or spleen (**H**) of mice with PGIA treated with vehicle (n = 11) and mice with PGIA treated with 5′-azaC (n = 12). Bars show the mean ± SEM. * = $P \leq 0.05$; ** = $P \leq 0.01$, *** = $P \leq 0.001$; **** = $P \leq 0.0001$, by the Mann-Whitney U test in **C** and **E** and by *t*-test in **D** and **F–H**. See Figure 1 for other definitions.

ies. Samples were collected before the first 5′-azaC treatment and when the experiment was terminated. IgM levels were enhanced in both animal groups, but IgG1 levels were increased only in vehicle-treated mice (Figures 2A and B). This suggested a compromised CSR (25,26) in 5′-azaC–treated mice. Hence, we measured IgG1-specific genome rearrangement in B cells using a modified version of digestion-circulation PCR (22). The level of class-switched DNA (Figure 2C) and the level of post-recombination IgG1 messenger RNA (mRNA) (Figure 2D) were significantly lower in 5′-azaC–treated mice. Since *Aicda* regulates CSR (26), we determined its expression level, which was significantly lower in 5′-azaC–treated animals (Figure 2E). These data suggest that 5′-azaC inhibits *Aicda* expression, leading to diminished CSR and attenuated antibody production in B cells, ultimately resulting in the suppression of arthritis symptoms.

Treatment with 5'-azaC inhibits GC formation and shifts the proportion of former B cell subpopulations in mice with PGIA. Self-reactive antibodies are mainly generated in GCs of secondary lymphoid organs (18). Thus, we investigated GC formation and determined the proportion of GC B cells in the mouse lymph nodes and spleen. Reduced GC formation and significantly decreased GC B cell frequency were observed in both organs in 5′-azaC–treated mice (Figures 3A–D and Supplementary Figures 1A and B, available on the *Arthritis & Rheumatology* web site at http://onlinelibrary.wiley.com/doi/10.1002/art.40877/abstract). Moreover, as a consequence of diminished GC formation, the proportion of plasma cells was also decreased in the BM of 5′-azaC–treated animals (Figure 3E and Supplementary Figure 1C).

To explore the origin of the altered frequency of GC B cells, we examined B cell subpopulations in mouse BM and spleen. In both organs, the proportions of B cells were significantly lower in the lymphocyte compartments in 5′-azaC–treated animals (Supplementary Figure 2, available on the *Arthritis & Rheumatology* web site at http://onlinelibrary.wiley.com/doi/10.1002/art.40877/abstract). The proportions of early precursor B cells were increased (Figure 3F), while the frequencies of late precursor (Figure 3F) and immature B cells (Figure 3G) were reduced upon 5′-azaC treatment. In the periphery, we detected a decreased proportion of transitional type 1 (T1) B cells, while the frequencies of follicle-colonizing T2 and marginal zone (MZ) B cells were elevated within the B cell populations of 5′-azaC–treated mice (Figure 3H). Finally, 5′-azaC treatment also elevated the percentage of the mature recirculating B cells in the BM (Figure 3G). The proportion of follicular B cells, which are essential in GC responses (18), was similar in the vehicle-treated and 5′-azaC–treated mice

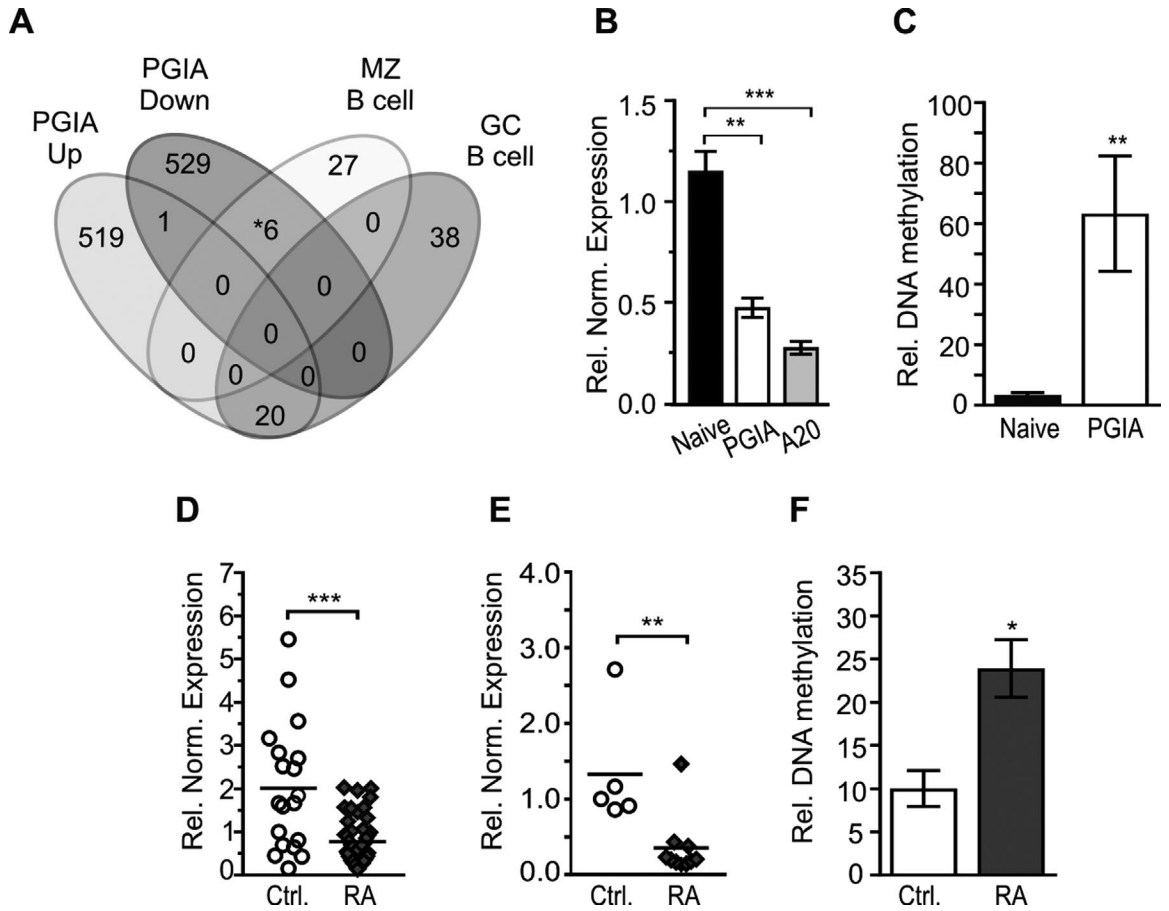

Figure 4. Hypermethylated *Ahr* regulatory regions in mice with PGIA and treatment-naive patients with rheumatoid arthritis (RA). **A**, Venn diagram of PGIA-associated (up-regulated and down-regulated), marginal zone (MZ)–specific, and germinal center (GC)–specific B cell genes. * = includes the *Ahr* gene. **B**, Relative (rel) normalized (norm) *Ahr* mRNA expression in splenic B cells from naive mice (n = 3), splenic B cells from mice with PGIA (n = 3), and in the mouse A20 B lymphoma cell line. **C**, Relative DNA methylation level of the *Ahr* promoter in splenic B cells from naive mice (n = 3) and mice with PGIA (n = 3). **D** and **E**, Relative normalized *AHR* mRNA expression in human peripheral blood mononuclear cells (PBMCs) isolated from healthy individuals (n = 19) and treatment-naive RA patients (n = 46) (**D**) and in human B cells isolated from healthy individuals (n = 5) and treatment-naive RA patients (n = 10) (**E**). **F**, Relative DNA methylation level of differentially methylated region C of *AHR* in PBMCs from healthy individuals (n = 10) and treatment-naive RA patients (n = 11). In **B**, **C**, and **F**, bars show the mean ± SEM. In **D** and **E**, symbols represent individual patients; horizontal lines show the mean. * = $P \leq 0.05$; ** = $P \leq 0.01$; *** = $P \leq 0.001$, by one-way ANOVA with Sidak's test in **B**, by *t*-test in **C,** and by the Mann-Whitney U test in **D–F**. See Figure 1 for other definitions.

with PGIA (Figure 3H and Supplementary Figure 3, available on the *Arthritis & Rheumatology* web site at http://onlinelibrary.wiley.com/doi/10.1002/art.40877/abstract).

Since follicular B cells can evolve GCs in a T cell–dependent manner (27), we investigated the frequency of CD4+ T cells and measured serum levels of IL-4 cytokine, which is predominantly produced by GC-forming follicular T helper cells (28). Interestingly, neither the frequency of CD4+ T cells nor the serum level of IL-4 was changed in 5′-azaC–treated mice compared to vehicle-treated arthritic animals (data not shown).

Hypermethylated *Ahr* regulatory regions in arthritic mouse B cells and human samples. DNA hypomethylation induced by 5′-azaC is nonspecific (29), in contrast to the locus-specific *Aicda*-mediated hypomethylation events in the B cell epigenome, which are essential for effective GC formation (17). Accordingly, it is conceivable that 5′-azaC–induced demethylation may provoke genes that inhibit GC formation. Taking this into account, our aim was to identify genes that could be induced by 5′-azaC and suppress *Aicda* expression. To this end, we compared arthritis-associated up-regulated and down-regulated genes (Figure 1A) with characteristic sets of MZ and GC B cell genes (30) (Figure 4A) that express *Aicda* (15,25). We focused on down-regulated genes that were also hypermethylated in arthritis, which can be possible targets of 5′-azaC–triggered activation (Supplementary Table 6, available on the *Arthritis & Rheumatology* web site at http://onlinelibrary.wiley.com/doi/10.1002/art.40877/abstract). These down-regulated genes included the *Ahr* gene, which encodes a transcription factor that is known to suppress *Aicda* expression after agonist stimulation (20). Indeed, *Ahr* expression was down-regulated (Figure 4B) and its promoter was hypermethylated in B cells isolated from mice with PGIA (Figure 4C and Supplementary Figure 4, available on the *Arthritis & Rheumatology* web site at http://onlinelibrary.wiley.com/doi/10.1002/art.40877/abstract).

Importantly, the disease specificity of down-regulated *AHR* expression was confirmed in PBMCs and B cells (Figures 4D and E) isolated from treatment-naive RA patients. RA-associated DNA hypermethylation was not observed in the *AHR* promoter region; however, a distant intergenic region (differentially methylated region C) 155 kb upstream of the *AHR* transcription start site (TSS) was differentially hypermethylated (Figure 4F and Supplementary Figure 5, available on the *Arthritis & Rheumatology* web site at http://onlinelibrary.wiley.com/doi/10.1002/art.40877/abstract). These results suggest that the *AHR* gene can be silenced in a DNA methylation–dependent manner and that *AHR* silencing may be involved in RA pathology.

Demethylation of the *Ahr* promoter plays a significant role in the inhibition of *Aicda*. To verify that 5′-azaC induced *Ahr* expression, we defined the promoter methylation and expression of *Ahr* in B cells. Indeed, *Ahr* promoter demethylation and accompanying elevated *Ahr* gene expression (Figures 5A and B) were identified in 5′-azaC–treated mice with PGIA. To determine the mechanistic connection between 5′-azaC–induced *Ahr* and *Aicda*, we conducted experiments with A20 cells, a BALB/c mouse B lymphoma cell line (31). In these cells, *Ahr* expression was down-regulated as in arthritic mouse B cells (Figure 4B). Furthermore, 5′-azaC treatment evoked a significant increase in *Ahr* expression (Figure 5C) due to its promoter demethylation (Figure 5D). Moreover, *Ahr* was translocated into the nucleus (Figure 5E), indicating its engagement in transcriptional regulation.

Next, to confirm the involvement of 5′-azaC–induced *Ahr* in down-regulated *Aicda* expression (Figures 5E and F), we used an shRNA-mediated inhibition approach. Treatment with 5′-azaC

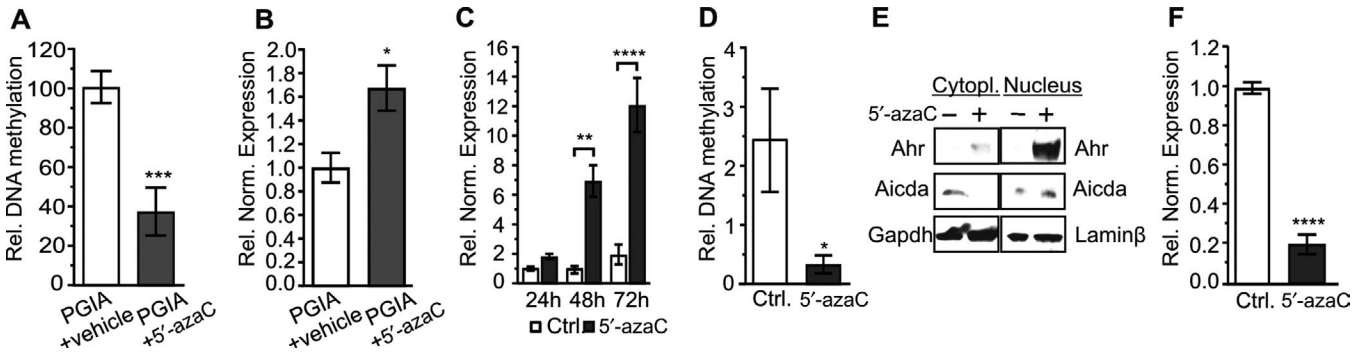

Figure 5. Demethylation induced by 5′-azaC provokes *Ahr* expression in vivo and in vitro. **A**, Relative (rel) DNA methylation level of the *Ahr* promoter in B cells from mice with PGIA treated with vehicle (n = 4) and mice with PGIA treated with 5′-azaC (n = 3). **B**, Relative normalized (norm) *Ahr* mRNA expression in B cells from mice with PGIA treated with vehicle (n = 8) and mice with PGIA treated with 5′-azaC (n = 8). **C** and **D**, Relative normalized *Ahr* mRNA expression in A20 cells after 24, 48, and 72 hours of treatment with 10 μ*M* 5′-azaC or 0.1% DMSO as control (**C**) and relative DNA methylation level of the *Ahr* promoter in A20 cells after 48 hours of treatment with 5′-azaC or control (**D**) (n = 3 samples per group). **E**, Localization of *Ahr* and *Aicda* in the cytoplasm and nucleus of A20 cells treated with 5′-azaC for 48 hours. GAPDH and lamin β were used as loading controls. **F**, Relative normalized *Aicda* mRNA expression in A20 cells treated with 5′-azaC or control for 48 hours (n = 3 samples per group). In **A–D** and **F**, bars show the mean ± SEM. * = $P \leq 0.05$; ** = $P \leq 0.01$; *** = $P \leq 0.001$; **** = $P \leq 0.0001$, by *t*-test in **A**, **B**, **D**, and **F** and by two-way ANOVA with Sidak's test in **C**. See Figure 1 for definitions.

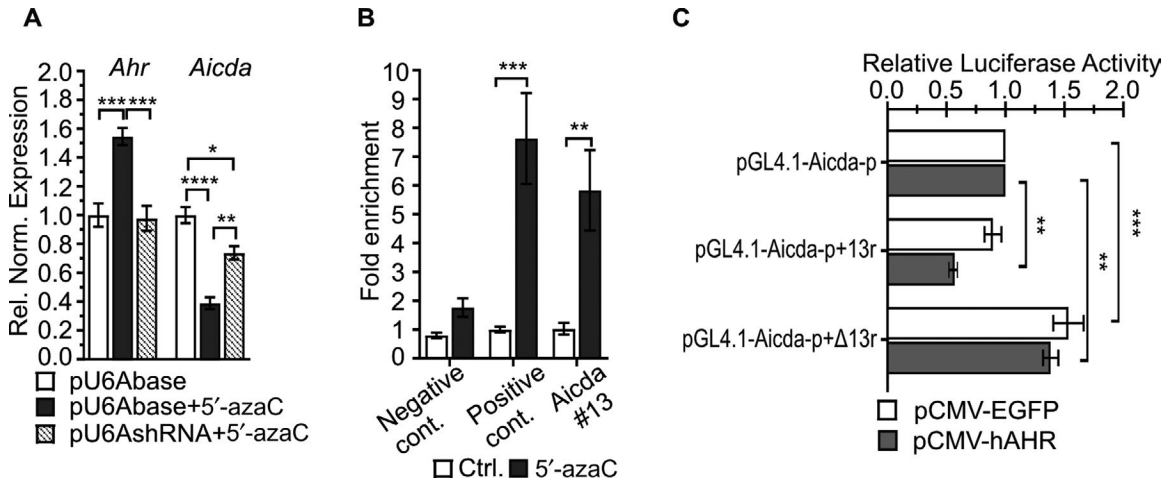

Figure 6. Direct regulation of *Aicda* by 5′-azaC–induced *Ahr*. **A,** Relative (rel) normalized (norm) *Ahr* and *Aicda* mRNA expression in A20 cells transfected with a control plasmid (pUTAbase) alone or transfected with an anti–*Ahr* short hairpin RNA (shRNA)–expressing plasmid (pU6AshRNA) or control plasmid and then treated with 5′-azaC for 48 hours (n = 3 samples per group). **B,** Chromatin immunoprecipitation analysis of *Ahr* binding to region 13 (Supplementary Table 4, available on the *Arthritis & Rheumatology* web site at http://onlinelibrary.wiley.com/doi/10.1002/art.40877/abstract) in the first intron of *Aicda* in A20 cells treated with 5′-azaC or control for 48 hours (n = 3 per group). The intergenic region was used as a negative control and the *CYP1a1* promoter region was used as a positive control. Data are presented as fold enrichment compared to the values for control treatment. **C**, Relative luciferase activity of the mouse *Aicda* promoter-driven reporter gene alone (pGL4.1-Aicda-p), the *Aicda* promoter-driven reporter gene with a segment of the first intron of *Aicda* including region 13 (pGL4.1-Aicda-p+13r), or the *Aicda* promoter-driven reporter gene with the same segment without region 13 (pGL4.1-Aicda-p+Δ13r). Reporter plasmids were cotransfected with a human *AHR*-expressing plasmid (pCMV-hAHR) or enhanced green fluorescent protein (EGFP)–expressing plasmid (pCMV-EGFP). Luciferase activity was normalized to cellular protein concentrations (n = 3 samples per group). Bars show the mean ± SEM. * = $P \leq 0.05$; ** = $P \leq 0.01$; *** = $P \leq 0.001$; **** = $P \leq 0.0001$, by two-way ANOVA with Sidak's test. See Figure 1 for other definitions.

did not increase *Ahr* expression when *Ahr*-specific shRNA was expressed in A20 cells, resulting in only a moderate decrease in *Aicda* expression (Figure 6A). Furthermore, we performed *Ahr*-specific ChIP focused on such regions (Supplementary Table 4, available on the *Arthritis & Rheumatology* web site at http://onlinelibrary.wiley.com/doi/10.1002/art.40877/abstract) in the genomic context of the *Aicda* gene that harbor in silico predicted *Ahr* binding sites (32). We detected 5′-azaC–induced *Ahr* binding in the first intron, termed region 13 (Figure 6B). Although region 13 does not contain a canonical *Ahr* binding site (33), it carries reasonably similar sequences to a ChIP-Seq–defined *Ahr* binding consensus motif (34), which was capable of binding *Ahr* effectively (Supplementary Figure 6, available on the *Arthritis & Rheumatology* web site at http://onlinelibrary.wiley.com/doi/10.1002/art.40877/abstract).

Finally, in transient expression studies, *AHR* only reduced the activity of an *Aicda* promoter-driven reporter gene if the inserted *Aicda* first intronic segment included region 13 (Figure 6C). These data demonstrate that *Ahr* bound directly to the regulatory region of *Aicda* after 5′-azaC treatment, but this region did not overlap with a previously described intronic silencer region (20). Our in vitro and in vivo experiments showed that 5′-azaC–induced demethylation rescues *Ahr* from hypermethylation-mediated down-regulation. B cell culture–based data demonstrated that reactivated *Ahr* directly contributed to the suppression of *Aicda* expression through a novel regulatory region in B cells. Therefore, it is plausible that the *Ahr–Aicda* regulatory cascade is responsible for attenuated GC formation and antibody production, which ultimately ameliorates arthritis symptoms.

DISCUSSION

Targeted inhibition of DNA methylation has already been proven to be an effective approach to restoring the expression of tumor suppressor genes and their cellular function (12). Herein we demonstrated that in vivo treatment with a DNA methyltransferase inhibitor has therapeutic potential in autoimmune arthritis as well.

We identified a number of differentially hypermethylated regions in arthritic mouse B cells (Figure 1A) and detected genome-wide hypomethylation, consistent with the findings of previous studies (35). However, the hypomethylation cannot be considered disease-specific because DNA demethylation also occurs during "normal" B cell maturation and activation (17,36–38). In contrast, disease-associated, less frequent hypermethylation events probably play more significant roles in arthritis etiology. This concept was supported by the findings of a study investigating fibroblast-like synoviocytes in RA patients (10) and an in vitro study of PBMCs from RA patients (13).

DNA demethylation induced by 5′-azaC halted arthritis progression in mice (Figures 1B and C), which can be attributed to the inhibited production of IgG1 antibodies (Figure 2B), since they can participate in joint destruction by forming immune complexes on the articular cartilage surface (39). Furthermore, high-affinity anti-

bodies, including self-reactive antibodies, are generated in GCs of secondary lymphoid organs (18) wherein CSR occurs due to high *Aicda* expression (25,26). Thus, the reduced *Aicda* expression and CSR, which ultimately lead to inhibited IgG1 production, can be attributed to the diminished GC formation in 5′-azaC–treated mice (Figures 3A and B).

To clarify the cause of the decrease in the proportion of GC B cells, we determined the frequencies of former B cell subpopulations. The frequencies of these subpopulations were similar to those previously found in anti-CD20–depleted mice (40). In light of the consistency of the findings, our results and those of the previous study can be explained in a similar way. The lower proportions of total B cells in the lymphocyte compartments after 5′-azaC treatment (Supplementary Figure 2, available on the *Arthritis & Rheumatology* web site at http://onlinelibrary.wiley.com/doi/10.1002/art.40877/abstract) induced a compensatory mechanism which is intended to sustain the constant frequency of follicular B cells and resulted in increased proportions of early precursor B cells (Figure 3F) (40) or follicular B cell–derived (41) mature recirculating B cells (Figure 3G). At the same time, a selective incident with a higher negative selection pressure could be induced, resulting in a decreased frequency of late precursor, immature (Figures 3F and G), and T1 B cells (Figure 3H) (42). Moreover, mature recirculating B cells constitute a reservoir for MZ B cells (41); thus, there might be a positive relationship between the increased frequencies of these cells (Figures 3G and H). Ultimately, these changes did not disturb the proportion of GC-forming (18) follicular B cells (Figure 3H). Taken together with an unchanged frequency of CD4+ T cells and serum IL-4 level, these data suggest that B cell intrinsic factors are the cause of diminished GC formation.

The contribution of *Ahr* to autoimmune arthritis has been investigated in two previous studies using the collagen-induced arthritis model. In the first study, *Ahr* altered T cell differentiation and promoted pathogenesis (43), while the other study showed that it exerted a preventive effect by inhibiting mesenchymal stem cell differentiation (44). Our findings are consistent with those of the latter study and demonstrate that DNA hypermethylation–mediated silencing of *Ahr* contributes to arthritis pathogenesis. This hypermethylated region is located in the *Ahr* promoter in arthritic mouse B cells (Figure 4C and Supplementary Figure 4, available on the *Arthritis & Rheumatology* web site at http://onlinelibrary.wiley.com/doi/10.1002/art.40877/abstract) or in a distant upstream region in RA patients (Supplementary Figure 5, available on the *Arthritis & Rheumatology* web site at http://onlinelibrary.wiley.com/doi/10.1002/art.40877/abstract). ChIP-Seq data demonstrate that transcription factors can bind to this distant region (45–47), suggesting that this region is a B cell–specific enhancer.

We demonstrated that 5′-azaC–induced demethylation could rescue *Ahr* from hypermethylation-related down-regulation (Figure 5B). This rescued *Ahr* contributed to the attenuated IgG1 production through the suppression of *Aicda* (Figure 5F), which is an essential regulator of GC formation (17). *Ahr* bound directly to the intronic regulatory region of *Aicda* after 5′-azaC treatment (Figure 6B), but this region did not overlap with a previously described silencer region in the first intron ~1.3 kb downstream from the TSS (20). This finding provides evidence of the existence of a different *Ahr* regulatory mechanism in 5′-azaC–treated arthritic B cells, which may come from distinct activation methods.

In summary, in this study, we demonstrated that 5′-azaC, a Food and Drug Administration–approved anticancer agent used for the treatment of various blood cell malignancies, effectively treats autoimmune arthritis when administered at low doses beginning at the early phase of the disease. Furthermore, we explored the notion that the beneficial effect of 5′-azaC is owed to compromised GC formation and subsequent reduced antibody production in which *Ahr* promoter demethylation can play a pivotal role. Our data provide a foundation for further studies exploring the therapeutic potential of low-dose DNA methyltransferase inhibitors in RA and other antibody-dependent diseases.

ACKNOWLEDGMENTS

We thank Ms. Szilvia Pördi for excellent technical assistance. We are indebted to Drs. Lionel Clement and Camille Mace (Rush University Medical Center) for the loan of a luminometer for luciferase assays.

AUTHOR CONTRIBUTIONS

All authors were involved in drafting the article or revising it critically for important intellectual content, and all authors approved the final version to be published. Dr. Rauch had full access to all of the data in the study and takes responsibility for the integrity of the data and the accuracy of the data analysis.

Study conception and design. Tóth, Glant, Rauch.

Acquisition of data. Tóth, Ocskó, Balog, Markovics, Jolly, Bukiej, Ruthberg, Rauch.

Analysis and interpretation of data. Tóth, Ocskó, Balog, Mikecz, Kovács, Vida, Block, Glant, Rauch.

REFERENCES

1. Zan H, Casali P. Epigenetics of peripheral B-cell differentiation and the antibody response. Front Immunol 2015;6:631.
2. Katchamart W, Trudeau J, Phumethum V, Bombardier C. Methotrexate monotherapy versus methotrexate combination therapy with non-biologic disease modifying anti-rheumatic drugs for rheumatoid arthritis. Cochrane Database Syst Rev 2010:CD008495.
3. GTEx Consortium. Genetic effects on gene expression across human tissues. Nature 2017;550:204–13.
4. Licht JD. DNA methylation inhibitors in cancer therapy: the immunity dimension. Cell 2015;162:938–9.
5. Bottini N, Firestein GS. Epigenetics in rheumatoid arthritis: a primer for rheumatologists. Curr Rheumatol Rep 2013;15:372.
6. Guillamot M, Cimmino L, Aifantis I. The impact of DNA methylation in hematopoietic malignancies. Trends Cancer 2016;2:70–83.
7. Karouzakis E, Gay RE, Michel BA, Gay S, Neidhart M. DNA hypomethylation in rheumatoid arthritis synovial fibroblasts. Arthritis Rheum 2009;60:3613–22.

8. Rauch TA, Zhong X, Wu X, Wang M, Kernstine KH, Wang Z, et al. High-resolution mapping of DNA hypermethylation and hypomethylation in lung cancer. Proc Natl Acad Sci U S A 2008;105:252–7.
9. Richardson B, Scheinbart L, Strahler J, Gross L, Hanash S, Johnson M. Evidence for impaired T cell DNA methylation in systemic lupus erythematosus and rheumatoid arthritis. Arthritis Rheum 1990;33:1665–73.
10. Maeshima K, Stanford SM, Hammaker D, Sacchetti C, Zeng L, Ai R, et al. Abnormal PTPN11 enhancer methylation promotes rheumatoid arthritis fibroblast-like synoviocyte aggressiveness and joint inflammation. JCI Insight 2016;1:e86580.
11. Gnyszka A, Jastrzębski Z, Flis S. DNA methyltransferase inhibitors and their emerging role in epigenetic therapy of cancer. Anticancer Res 2013;33:2989–96.
12. Scott LJ. Azacitidine: a review in myelodysplastic syndromes and acute myeloid leukaemia. Drugs 2016;76:899–900.
13. Fu LH, Ma CL, Cong B, Li SJ, Chen HY, Zhang JG. Hypomethylation of proximal CpG motif of interleukin-10 promoter regulates its expression in human rheumatoid arthritis. Acta Pharmacol Sin 2011;32:1373–80.
14. Glant TT, Cs-Szabó G, Nagase H, Jacobs JJ, Mikecz K. Progressive polyarthritis induced in BALB/c mice by aggrecan from normal and osteoarthritic human cartilage. Arthritis Rheum 1998;41:1007–18.
15. Cerutti A, Cols M, Puga I. Marginal zone B cells: virtues of innate-like antibody-producing lymphocytes. Nat Rev Immunol 2013;13:118–32.
16. Mesin L, Ersching J, Victora GD. Germinal center B cell dynamics. Immunity 2016;45:471–82.
17. Dominguez PM, Teater M, Chambwe N, Kormaksson M, Redmond D, Ishii J, et al. DNA methylation dynamics of germinal center B cells are mediated by AID. Cell Rep 2015;12:2086–98.
18. DeFranco AL. Germinal centers and autoimmune disease in humans and mice. Immunol Cell Biol 2016;94:918–24.
19. Stockinger B, Di Meglio P, Gialitakis M, Duarte JH. The aryl hydrocarbon receptor: multitasking in the immune system. Annu Rev Immunol 2014;32:403–32.
20. Vaidyanathan B, Chaudhry A, Yewdell WT, Angeletti D, Yen WF, Wheatley AK, et al. The aryl hydrocarbon receptor controls cell-fate decisions in B cells. J Exp Med 2017;214:197–208.
21. Glant TT, Mikecz K, Arzoumanian A, Poole AR. Proteoglycan-induced arthritis in BALB/c mice: clinical features and histopathology. Arthritis Rheum 1987;30:201–12.
22. Lumsden JM, McCarty T, Petiniot LK, Shen R, Barlow C, Wynn TA, et al. Immunoglobulin class switch recombination is impaired in ATM-deficient mice. J Exp Med 2004;200:1111–21.
23. Tóth DM, Szoke É, Bölcskei K, Kvell K, Bender B, Bosze Z, et al. Nociception, neurogenic inflammation and thermoregulation in TRPV1 knockdown transgenic mice. Cell Mol Life Sci 2011;68:2589–601.
24. Arribas AJ, Bertoni F. Methylation patterns in marginal zone lymphoma. Best Pract Res Clin Haematol 2017;30:24–31.
25. Stavnezer J, Guikema JE, Schrader CE. Mechanism and regulation of class switch recombination. Annu Rev Immunol 2008;26:261–92.
26. Stavnezer J. Complex regulation and function of activation-induced cytidine deaminase. Trends Immunol 2011;32:194–201.
27. Kleiman E, Salyakina D, De Heusch M, Hoek KL, Llanes JM, Castro I, et al. Distinct transcriptomic features are associated with transitional and mature B-cell populations in the mouse spleen. Front Immunol 2015;6:30.
28. Crotty S. Follicular helper CD4 T cells (TFH). Annu Rev Immunol 2011;29:621–63.
29. Grövdal M, Karimi M, Tobiasson M, Reinius L, Jansson M, Ekwall K, et al. Azacitidine induces profound genome-wide hypomethylation in primary myelodysplastic bone marrow cultures but may also reduce histone acetylation. Leukemia 2014;28:411–3.
30. Mabbott NA, Gray D. Identification of co-expressed gene signatures in mouse B1, marginal zone and B2 B-cell populations. Immunology 2014;141:79–95.
31. Bhattacharya P, Grigera F, Rogozin IB, McCarty T, Morse HC, Kenter AL. Identification of murine B cell lines that undergo somatic hypermutation focused to A:T and G:C residues. Eur J Immunol 2008;38:227–39.
32. Mathelier A, Fornes O, Arenillas DJ, Chen CY, Denay G, Lee J, et al. JASPAR 2016: a major expansion and update of the open-access database of transcription factor binding profiles. Nucleic Acids Res 2016;44:D110–5.
33. Swanson HI, Chan WK, Bradfield CA. DNA binding specificities and pairing rules of the Ah receptor, ARNT, and SIM proteins. J Biol Chem 1995;270:26292–302.
34. Lo R, Matthews J. High-resolution genome-wide mapping of AHR and ARNT binding sites by ChIP-Seq. Toxicol Sci 2012;130:349–61.
35. Liu Y, Aryee MJ, Padyukov L, Fallin MD, Hesselberg E, Runarsson A, et al. Epigenome-wide association data implicate DNA methylation as an intermediary of genetic risk in rheumatoid arthritis. Nat Biotechnol 2013;31:142–7.
36. Kulis M, Merkel A, Heath S, Queirós AC, Schuyler RP, Castellano G, et al. Whole-genome fingerprint of the DNA methylome during human B cell differentiation. Nat Genet 2015;47:746–56.
37. Oakes CC, Seifert M, Assenov Y, Gu L, Przekopowitz M, Ruppert AS, et al. DNA methylation dynamics during B cell maturation underlie a continuum of disease phenotypes in chronic lymphocytic leukemia. Nat Genet 2016;48:253–64.
38. Lai AY, Mav D, Shah R, Grimm SA, Phadke D, Hatzi K, et al. DNA methylation profiling in human B cells reveals immune regulatory elements and epigenetic plasticity at Alu elements during B-cell activation. Genome Res 2013;23:2030–41.
39. Anquetil F, Clavel C, Offer G, Serre G, Sebbag M. IgM and IgA rheumatoid factors purified from rheumatoid arthritis sera boost the Fc receptor– and complement-dependent effector functions of the disease-specific anti–citrullinated protein autoantibodies. J Immunol 2015;194:3664–74.
40. Shahaf G, Zisman-Rozen S, Benhamou D, Melamed D, Mehr R. B cell development in the bone marrow is regulated by homeostatic feedback exerted by mature B cells. Front Immunol 2016;7:77.
41. Cariappa A, Boboila C, Moran ST, Liu H, Shi HN, Pillai S. The recirculating B cell pool contains two functionally distinct, long-lived, posttransitional, follicular B cell populations. J Immunol 2007;179:2270–81.
42. Chung JB, Silverman M, Monroe JG. Transitional B cells: step by step towards immune competence. Trends Immunol 2003;24:343–9.
43. Nakahama T, Kimura A, Nguyen NT, Chinen I, Hanieh H, Nohara K, et al. Aryl hydrocarbon receptor deficiency in T cells suppresses the development of collagen-induced arthritis. Proc Natl Acad Sci U S A 2011;108:14222–7.
44. Tong Y, Niu M, Du Y, Mei W, Cao W, Dou Y, et al. Aryl hydrocarbon receptor suppresses the osteogenesis of mesenchymal stem cells in collagen-induced arthritic mice through the inhibition of β-catenin. Exp Cell Res 2017;350:349–57.
45. Ding C, Chen X, Dascani P, Hu X, Bolli R, Zhang H, et al. STAT3 signaling in B cells is critical for germinal center maintenance and contributes to the pathogenesis of murine models of lupus. J Immunol 2016;196:4477–86.
46. Gustems M, Woellmer A, Rothbauer U, Eck SH, Wieland T, Lutter D, et al. C-Jun/c-Fos heterodimers regulate cellular genes via a newly identified class of methylated DNA sequence motifs. Nucleic Acids Res 2014;42:3059–72.
47. Heavey B, Charalambous C, Cobaleda C, Busslinger M. Myeloid lineage switch of Pax5 mutant but not wild-type B cell progenitors by C/EBPα and GATA factors. EMBO J 2003;22:3887–97.